Imaging and focusing properties of plasmonic metamaterial devices

Igor I. Smolyaninov, Yu-Ju Hung, and Christopher C. Davis
Department of Electrical and Computer Engineering, University of Maryland, College Park, Maryland 20742, USA
(Received 9 July 2007; revised manuscript received 19 September 2007; published 20 November 2007)

Imaging and focusing devices based on negative refractive index behavior of surface plasmon polaritons are described. These devices are based on two-dimensional plasmonic metamaterials consisting of alternating layers of positive and negative refractive indices, which are arranged in either layered or checkerboard fashion on the surface of a gold film.

DOI: 10.1103/PhysRevB.76.205424 PACS number(s): 78.67.−n, 42.70.−a

I. INTRODUCTION

Current progress in nanotechnology and microbiology requires optical imaging and lithographical techniques with ever increasing spatial resolution. However, the spatial resolution of conventional optical devices is limited by the diffraction of light waves to a value of the order of 200 nm. Thus, viruses, proteins, DNA molecules, and many other samples are impossible to visualize using a regular optical microscope. The new ways to overcome this limitation may be based on the concept of superlens introduced by Pendry.[1] This concept relies on the use of materials which have negative refractive index in the visible frequency range. Even though superlens imaging has been demonstrated in the experiment,[2,3] until recently, this technique was limited by the fact that magnification of the planar superlens is equal to 1.

An important early step to overcome this limitation was made in surface plasmon-assisted microscopy experiments,[4] in which two-dimensional (2D) image magnification has been achieved. The increased spatial resolution of microscopy experiments performed with surface plasmon polaritons[5] is based on the "hyperbolic" dispersion law of such waves, which may be written in the form

$$k_{xy}^2 - |k_z|^2 = \frac{\epsilon_d \omega^2}{c^2}, \tag{1}$$

where ϵ_d is the dielectic constant of the medium bounding metal surface, $k_{xy}=k_p$ is the wave vector component in the plane of propagation, and k_z is the wave vector component perpendicular to the plane. This form of the dispersion relation originates from the exponential decay of the surface wave field away from the propagation plane. Negative refractive index behavior of surface plasmons was also shown to play a very important role in these early experiments.[6]

On the theoretical side, various new geometries exhibiting image magnification beyond the usual diffraction limit were proposed,[7–9] which make use of various metamaterial arrangements. For example, in the "optical hyperlens" design,[8] a concentric arrangement of metal and dielectric cylinders may be characterized by a strongly anisotropic dielectric permittivity tensor in which the tangential ϵ_θ and radial ϵ_r components have opposite signs. The resulting hyperbolic dispersion relation,

$$\frac{k_r^2}{\epsilon_\theta} - \frac{k_\theta^2}{|\epsilon_r|} = \frac{\omega^2}{c^2}, \tag{2}$$

does not exhibit any lower limit on the wavelength of propagating light at a given frequency. Thus, similar to the 2D optics of surface plasmon polaritons, there is no usual diffraction limit in this medium. The resolution is defined only by propagation losses. Following these theoretical ideas, magnifying superlenses (or hyperlenses) were independently realized in two experiments.[10,11] Far-field optical resolution of the order of 70 nm has been demonstrated using a magnifying superlens based on a 2D plasmonic metamaterial design.[10]

Our approach to design and fabrication of 2D plasmonic metamaterials is based on unusual optics of surface plasmon polaritons (SPPs). The properties of these two-dimensional optical modes and the convenient ways to excite them are described in detail in Ref. 5. The wave vector of SPPs propagating over a metal-dielectric interface is defined by the expression

$$k_p = \frac{\omega}{c}\left(\frac{\epsilon_d \epsilon_m}{\epsilon_d + \epsilon_m}\right)^{1/2}, \tag{3}$$

where $\epsilon_m(\omega)$ and $\epsilon_d(\omega)$ are the frequency-dependent dielectric constants of the metal and dielectric, respectively. Above the resonant frequency described by the condition

$$\epsilon_m(\omega) \approx -\epsilon_d(\omega), \tag{4}$$

the SPP group and phase velocities may have opposite signs. This behavior is illustrated in Fig. 1(a), which shows the SPP dispersion law for the cases of gold/vacuum and gold/polymethyl methacrylate (PMMA) interfaces. If a plasmon refraction experiment is conducted in the frequency range marked by a box in Fig. 1(a) in the 2D geometry shown in Fig. 1(b), an analysis based on energy and momentum conservation indicates that negative group velocity necessarily corresponds to negative 2D refraction index without any "optical magnetism" being involved. Thus, regular optical materials deposited onto gold film surface may be perceived by SPPs as negative refractive index materials. It is also important to note that according to Fig. 1(a), the figure of merit $\mathrm{Re}(k)/\mathrm{Im}(k)$ of these 2D negative index materials may reach the values of the order of 10. This relatively high value compared to the typical figures of merit of the three-dimensional (3D) negative index materials[12] makes possible

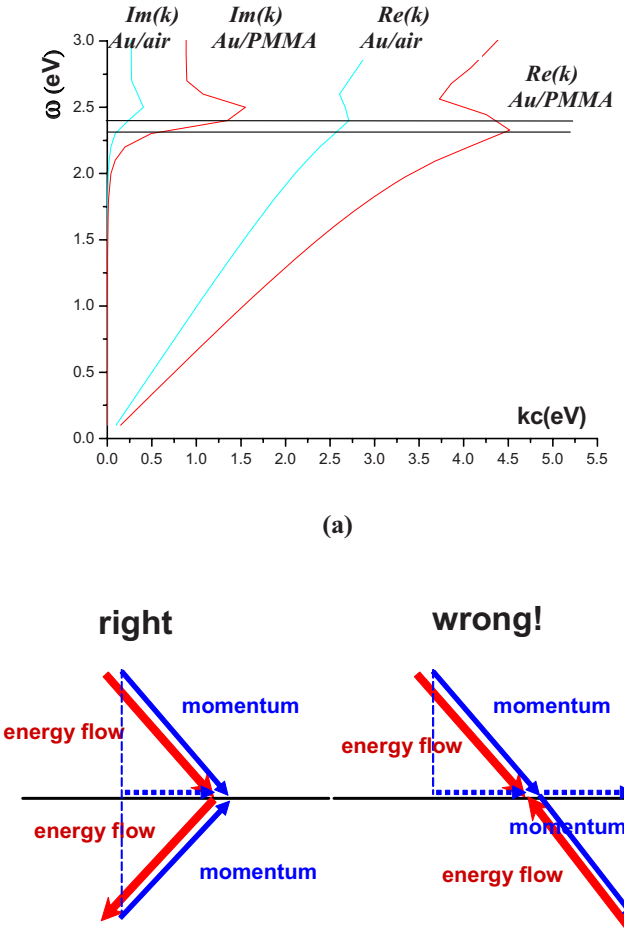

FIG. 1. (Color online) (a) Real Re(k) and imaginary Im(k) parts of the surface plasmon wave vector at the gold/polymethyl methacrylate (PMMA) and gold/vacuum interfaces as a function of frequency. In the frequency range marked by the box, PMMA has negative refractive index as perceived by plasmons, while gold/vacuum interface looks like a medium with positive refractive index. (b) A 2D refraction experiment: momentum conservation requires the projections of momenta to be the same in the incident and refracted waves. If a negative group velocity wave would refract in the "usual" positive direction, accumulation of energy near the interface would occur.

to use the 2D plasmonic metamaterials in practically useful optical devices.

A magnifying superlens originally presented in Ref. 10 is one example of such devices. The internal structure of the magnifying superlens is shown in Fig. 2(a). It consists of the concentric PMMA rings deposited on the gold film surface. Due to periodicity of the structure in the radial direction, SPPs are excited on the lens surface when the lens is illuminated with an external laser. In the frequency range marked by the box in Fig. 1(a), PMMA has negative refractive index $n_2<0$ as perceived by SPPs. The width of the PMMA rings d_2 may be chosen at will. If d_2 is chosen so that

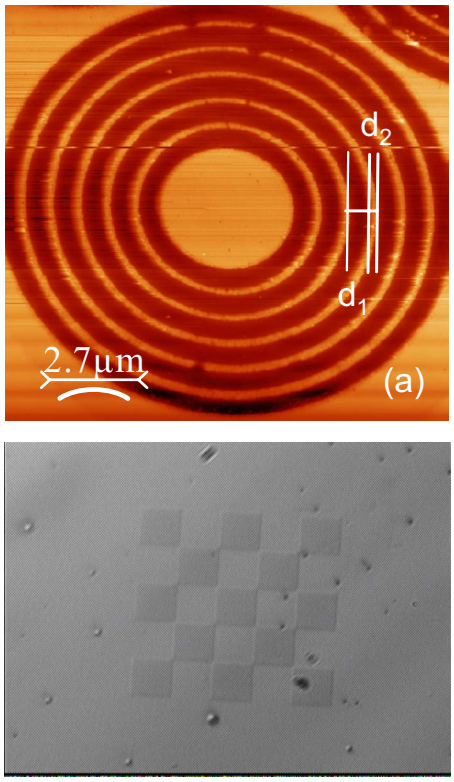

FIG. 2. (Color online) (a) AFM image of the magnifying superlens made of PMMA rings on the gold film surface. (b) An image of a checkerboard metamaterial device obtained using a regular optical microscope.

$n_1d_1=-n_2d_2$, where d_1 is the width of the gold/vacuum portions of the interface, the average optical width of the structure in the radial direction is zero. Thus, the local average refractive index of the structure may be varied continuously between n_1 and n_2 through zero by adjusting the geometrical parameters. The frequently discussed checkerboard metamaterials[13] in which individual squares exhibit alternating pattern of positive and negative refractive indices are also very easy to make using the same approach [Fig. 2(b)].

In this paper, we present a detailed account of imaging and focusing experiments performed with plasmonic metamaterial devices based on the principle described above. We are going to describe imaging experiments conducted using a magnifying superlens structure, and describe 2D focusing properties of parabolic surface grating, which may be very useful in one- and two-photon fluorescence imagings. Finally, we are going to describe our observations of subwavelength plasmonic cavities formed in the nodes of the checkerboard metamaterial structures.

II. EXPERIMENTAL RESULTS

Figure 3 demonstrates negative refraction in a layered 2D plasmonic material described above. Rows of dots have been produced in PMMA film near the edge of the layered material [see the atomic force microscopy (AFM) image in Fig.

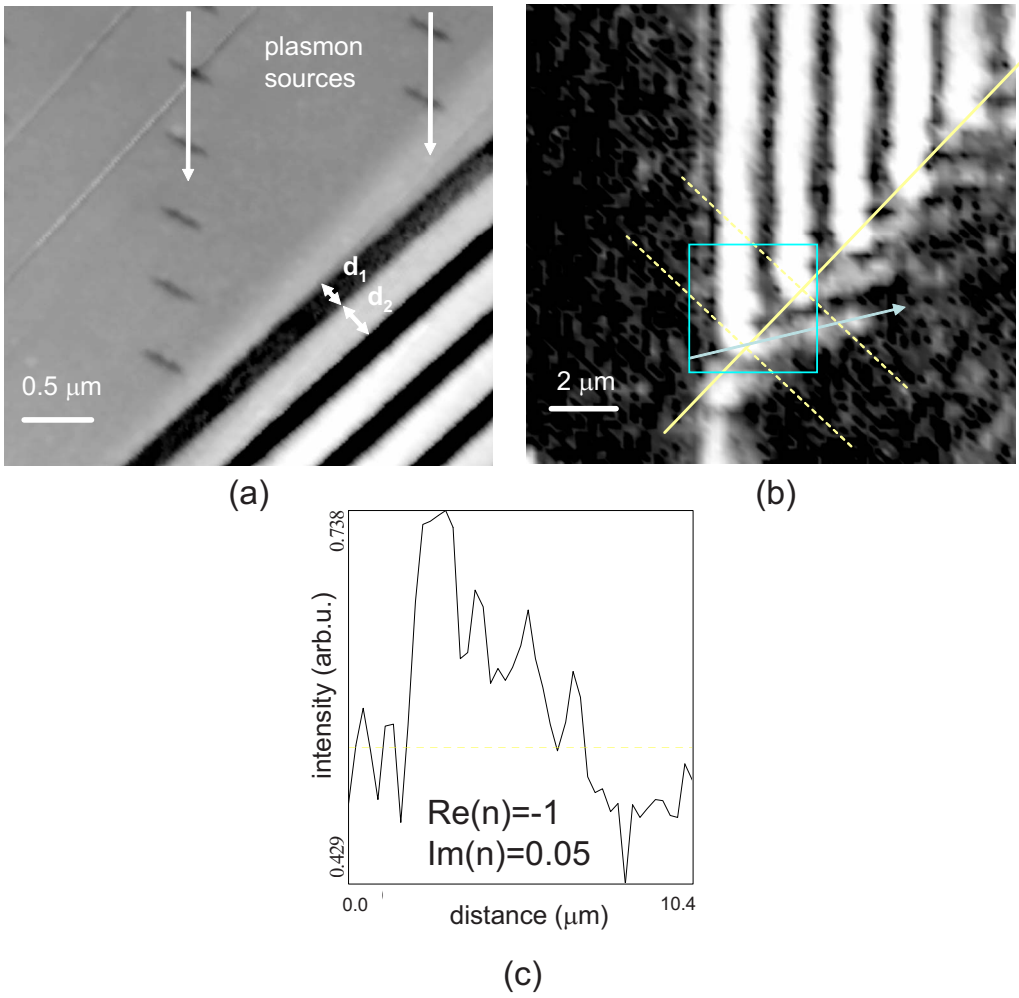

FIG. 3. (Color online) (a) AFM image of the test structure demonstrating the negative refractive index behavior of a layered 2D plasmonic material. The rows of defects generate plasmon rays when illuminated with a phase-matched laser light. (b) Optical image of the test structure demonstrates negative refraction of the plasmon rays. The boundary of the layered material is shown by the yellow line. The direction of one of the refracted rays is shown by the gray arrow. The relative position of the area shown in (a) is marked by a box. (c) Cross section of the optical image in (b) demonstrates attenuation of the refracted plasmon rays away from the boundary of the layered material. The data in (b) and (c) allow measurements of the complex refractive index of the layered plasmonic material.

3(a)]. The 0.5 μm periodicity of dots in these rows helps us to achieve phase matching between the incident laser light and surface plasmons. Upon illumination with an external laser, these rows of dots gave rise to the plasmon "rays" propagating in the direction shown by the arrows in Fig. 3(a). These rays are clearly visible in the optical image in Fig. 3(b) obtained using a conventional optical microscope. The incident plasmon rays give rise to the rays refracted in the negative direction at the boundary of the layered material. The propagation direction of the refracted rays corresponds to $\mathrm{Re}(n_{av})=-1$. The imaginary part of the effective refractive index is estimated to be $\mathrm{Im}(n_{av})=0.05$ from the exponential fit of the measured intensity attenuation of the refracted rays away from the boundary of the layered material. A typical line section of Fig. 3(b) along the propagation direction of one refracted ray is shown in Fig. 3(c) [this ray is chosen so that the line section would not intersect with the other incoming plasmon rays passing on the left, while its visible propagation length is about average among the five refracted rays visible in Fig. 3(b)]. While the negatively refracted rays visible in Fig. 3(b) exhibit some variations in brightness and visible propagation length, which is unavoidable in experiment, they all show about the same rate of exponential decay, which produced the $\mathrm{Im}(n_{av})=0.05$ estimate. Note that the magnitude of $\mathrm{Im}(n_{av})$ is consistent with the order of magnitude of the imaginary part of the surface plasmon wave vector in the experimental range, as shown in Fig. 1(a). We should emphasize that this result represents an order of magnitude improvement of the figure of merit $\mathrm{Re}(n_{av})/\mathrm{Im}(n_{av})$ of a negative refractive index material operating in the visible frequency range compared to the current state of the art.[12]

While imaging action of the magnifying superlens is based on the original superlens idea by Pendry[1] [Fig. 4(a)], its magnification is based on the fact that all the rays in the concentric multilayer superlens structure tend to propagate in the radial direction when $n_1 d_1 = -n_2 d_2$. This behavior is easy to illustrate using the ray optics approximation [Fig. 4(b)].

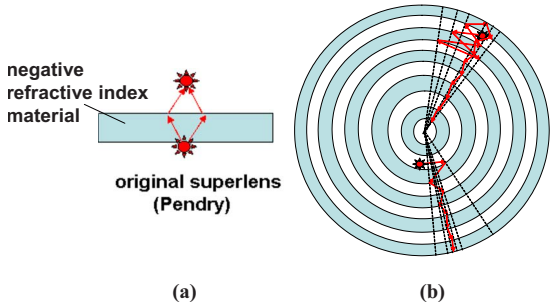

FIG. 4. (Color online) (a) Schematic view of superlens imaging. (b) All the rays in the concentric mulilayer superlens structure tend to propagate in the radial direction when $n_1 d_1 = -n_2 d_2$.

The geometry of imaging experiments using a magnifying superlens is shown in Fig. 5. The magnifying action of the superlens is demonstrated in Fig. 6(a), which presents the results of two actual imaging experiments [top portion of Fig. 6(a)] performed simultaneously with four control experiments seen at the bottom of the same image. An additional control experiment performed with the same structures fabricated on a glass slide coated with indium tin oxide (ITO) film (instead of a gold film as in Fig. 6) is presented in Fig. 7.

In these experiments, two rows of PMMA dots have been produced near the inner ring of the superlens structures seen at the top and at the bottom of Fig. 6(a), as shown in the AFM image in Fig. 6(b). These rows of PMMA dots had 0.5 μm periodicity in the radial direction so that phase matching between the incident 532 nm laser light and surface plasmons can be achieved. On the other hand, no such PMMA dot structure was fabricated near the control superlenses seen in the center of Fig. 6(a). Upon illumination with an external laser, the two rows of PMMA dots in Fig. 6(b) gave rise to the two divergent "plasmon rays," which are clearly visible in the top portion of the image in Fig. 6(a) obtained using a conventional optical microscope. No such rays were observed in the four "control" superlenses visible in the bottom portion of the same image. There was no sample to image for the two superlenses located in the center of Fig. 6(a). On the other hand, the PMMA dot structure was designed for phase-matched plasmon generation in the "upward" direction as seen in the image. That is why no plasmon rays are visible when the superlens structures are inverted, as seen in the bottom of Fig. 6(a). When the gold film is replaced with an ITO film in the same experimental geometry, no superlens imaging occurs (Fig. 7) since no surface plasmons are generated on ITO surface. The image in Fig. 7

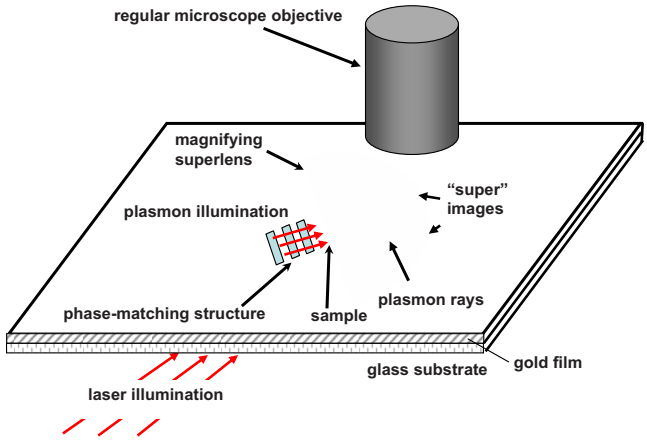

FIG. 5. (Color online) Schematic view of the magnifying superlens integrated into a conventional microscope. The plasmons generated by the phase-matching structure illuminate the sample positioned near the center of the superlens. The lateral distance between the images produced by the alternating layers of positive and negative refractive index materials grows with distance along the radius. The images are viewed by a regular microscope due to plasmon scattering into photons by the ridges of the PMMA rings.

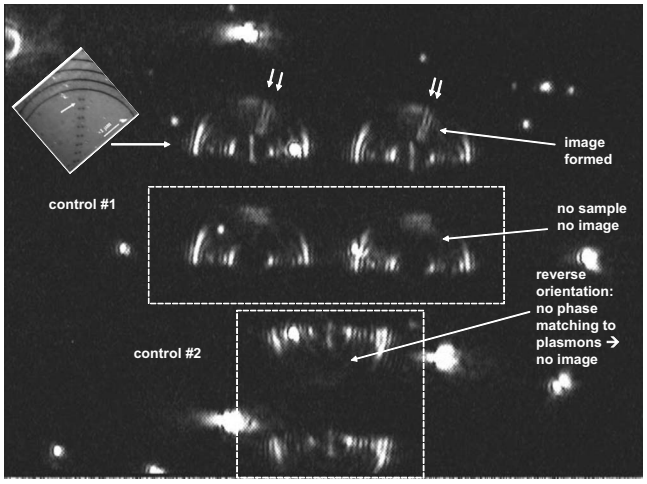

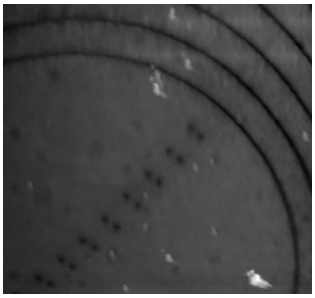

FIG. 6. (a) This image obtained using a conventional optical microscope presents the results of two imaging experiments (top portion of the image) performed simultaneously with four control experiments seen at the bottom of the same image. The rows of PMMA dots shown in the inset and in the AFM image (b) were fabricated near the two top and two bottom superlenses. No such pattern was made near the two superlenses visible in the center of the image. Upon illumination with an external laser, the two rows of PMMA dots separated by 130 nm gap gave rise to two divergent plasmon rays shown by the arrows, which are clearly visible in the top portion of the image. The four control superlenses visible at the bottom do not produce such rays because there is no sample to image for the two superlenses in the center, and the two bottom superlenses are inverted.

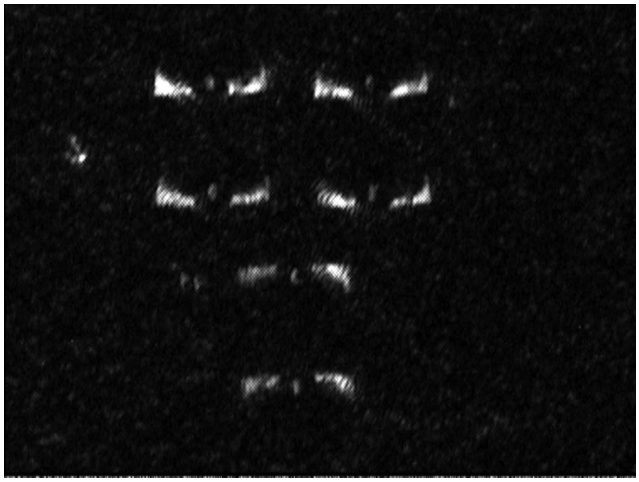

FIG. 7. Same pattern produced on ITO instead of gold film demonstrates the pattern of ordinary light scattering by the structure.

represents a pattern of regular light scattering by the test structure with the same geometry.

The cross-sectional analysis of the image in Fig. 6(a) across the plasmon rays (Fig. 8) indicates a resolution of at least 70 nm or $\lambda/7$. The lateral separation between these rays increased by a factor of 10 as the rays reached the outer rim of the superlens. This increase allowed visualization of the PMMA doublet using a conventional microscope. Comparison of Fig. 8(a) with the cross-sectional analysis of the AFM image of the doublets in Fig. 8(b) indicates that at present, the resolution of our imaging experiments is defined by the resolution of test sample fabrication. The actual optical resolution may be considerably better as suggested by the theoretical analysis performed in Ref. 8. An optical microscope based on the described imaging principle has the potential to become a useful tool in medical and biological imagings, where far-field optical imaging of individual viruses and DNA molecules may become a reality.

A slight change in experimental geometry helps us to convert the original superlens structure into an efficient 2D focusing device, as shown in Fig. 9. Instead of circular grating structure, a confocal parabolic grating geometry has been used. An array of four plasmon focusing devices shown in Figs. 9(a) and 9(b) was illuminated from the top by an external laser operating at 532 nm. The chosen illumination angle and the periodicity of the focusing devices correspond to the phase-matching excitation of SPPs counterpropagating in both left-to-right and right-to-left directions. A good degree of focusing has been observed, which may be explained by the fact that by design, the structure may operate as a 2D focusing device as both "plasmon mirror" and "plasmon lens" simultaneously [see the ray optics simulation shown in Fig. 9(c)]. It is interesting to note that a two-lens combination shown in Fig. 9(c) becomes a stable resonator if losses are neglected. This is illustrated by the ray optics simulation. However, the plasmon losses in the real structures shown in Figs. 9(a) and 9(b) are probably too high for the device to operate as a resonator.

Considerable theoretical efforts are also devoted for the understanding of the imaging and resonant properties of checkerboard structures consisting of negative and positive refractive index materials (see Ref. 13 as an example). Due to the ease of fabrication of such structures in 2D using the same PMMA lithography technique [Fig. 2(b)], these theo-

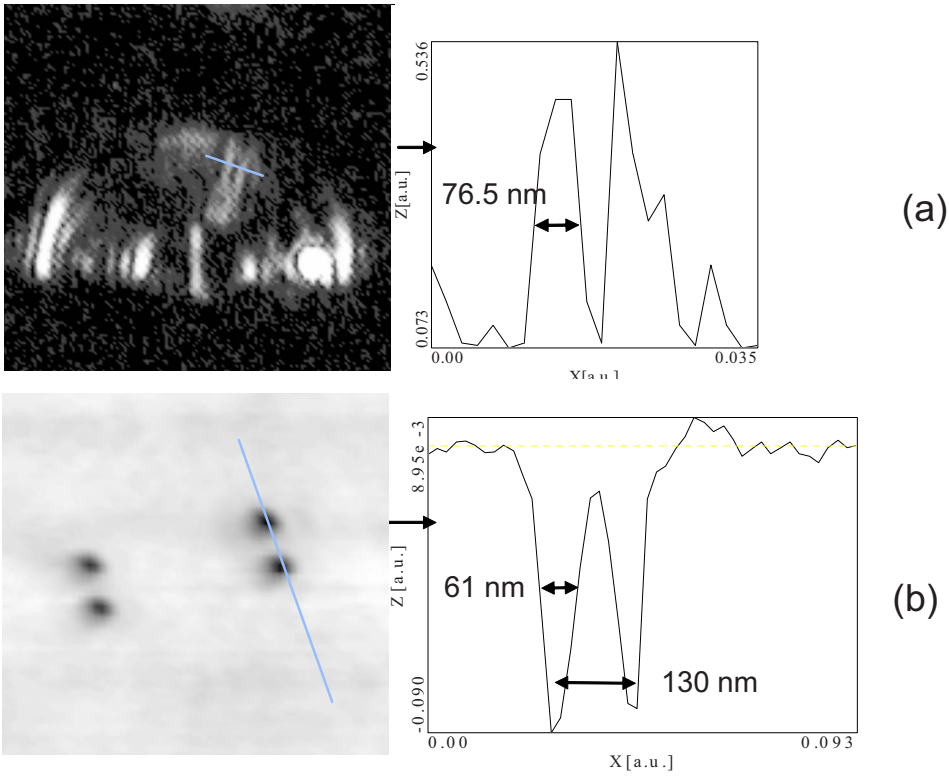

FIG. 8. (Color online) Cross-sectional analyses of (a) the plasmon rays from Fig. 5(a) and the AFM image of the test PMMA doublets from Fig. 5(b).

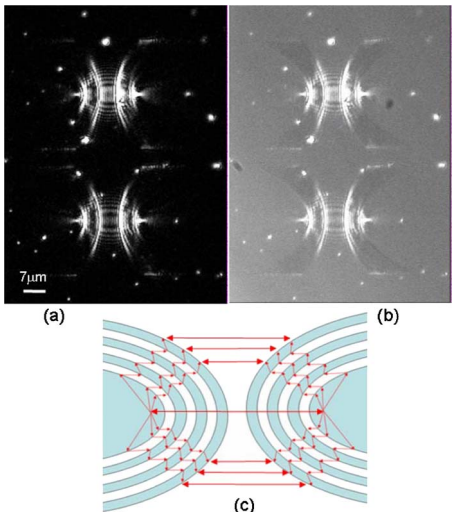

FIG. 9. (Color online) [(a) and (b)] Optical images of two 2D focusing devices based on the layered plasmonic material. (c) Ray optics illustration of the operating principle of the device. Negative refraction areas are shown in gray. It is interesting to note that such a two-lens combination becomes a stable resonator if losses are neglected.

retical efforts may be confronted with experiments. Figure 10(a) illustrates the formation of highly unusual optical cavities around the corners of the checkerboard structure using the ray optics approximation. A surface plasmon ray which propagates near the corner in any direction gets trapped in a stable trajectory rotating around the corner. It is interesting to note that the optical length of this cavity is equal to zero. Potentially, such cavities may be used to make compact subwavelength lasers, since the propagation losses in the cavity may be made quite small if the ray trajectory is located close to the corner. Figures 10(b) and 10(c) demonstrate optical images of a checkerboard pattern consisting of gold or PMMA and gold or air interfaces illuminated with either 502 or 632 nm laser light. Large periodicity of the structure cannot provide efficient phase matching to surface plasmon polaritons in this case. On the other hand, scattering of external light by edges of the checkerboard structure leads to SPP excitation.[5] The inner corners of the checkerboard structure exhibit very strong light scattering when illuminated by 502 nm light, which may be explained by the plasmons trapped in the corner cavities. On the other hand, the outer corners of the checkerboard structure exhibit considerably weaker light scattering. Magnified image of one square of the checkerboard pattern illuminated with *p*-polarized 502 nm laser light demonstrates the fourfold symmetry of optical intensity near each corner. This fourfold symmetry of light distribution in a checkerboard structure has been predicted by theoretical calculations (see, for example, Fig. 4 from Ref. 14). The observed effect depends strongly on the wavelength and the polarization state of the illuminating light. The scattered light intensity peaks strongly at 502 nm [see Figs. 10(b), 10(c), 10(e), and 10(f)]. The light scattered from the corners of the checkerboard structure is polarized

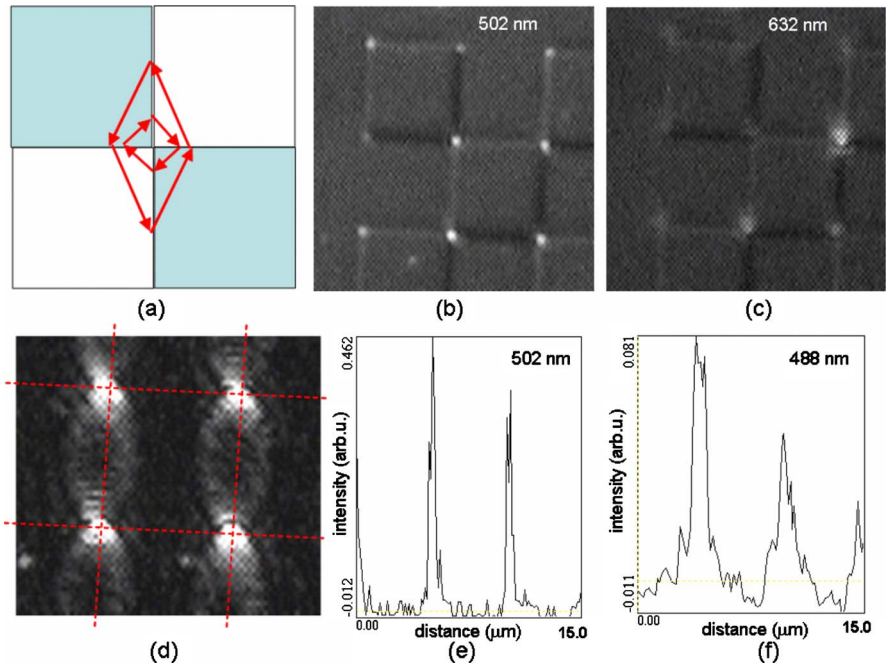

FIG. 10. (Color online) (a) Ray optics illustration of an optical cavity formed around the corner of a checkerboard refractive index structure. Negative refractive index areas are shown in gray. (b) Optical image of a checkerboard pattern (5 μm on a side) consisting of gold or PMMA and gold or air interfaces illuminated with *p*-polarized 502 nm laser light. The corners of the checkerboard structure exhibit strong light scattering, which may be explained by the cavities shown in (a). (c) Optical image of the same pattern illuminated with 632 nm laser light of the same polarization and power. (d) Magnified image of one square of the checkerboard pattern illuminated with *p*-polarized 502 nm laser light demonstrates the fourfold symmetry of optical intensity near each corner. (e) and (f) demonstrate the cross sections of optical intensity measured at 502 and 488 nm, respectively, using the same excitation optical power and polarization.

mostly in the *p* direction so that the field of view appears to be completely dark when *s* polarization is used for observations at the same power of the illuminating light. This is a direct indication of the important role of surface plasmon corner cavities in the observed phenomenon.

We should also note that the checkerboard cavity described above may be alternatively considered as a 2D analog of the bow tie antenna (see, for example, Ref. 15). As has been indicated in Ref. 16, in the zero loss limit above the surface plasmon resonance frequency defined by Eq. (4), a dielectric layer on top of a metal film behaves as a 2D analog of a metal. Hence, SPPs perceive the corners of the checkerboard structure in the same way as photons would perceive a sharp pair of metal corners.

III. CONCLUSION

While fabrication of three-dimensional photonic metamaterials faces numerous technological challenges, many concepts and ideas in the optics of metamaterials may be tested much easier in two spatial dimensions using planar optics of surface plasmon polaritons. Changing the geometry and composition of multilayers in SPP-based metamaterials will be very important to metamaterial researches in that it can provide experimental verification of many nanophotonic devices in the optical frequency range. We have presented various examples of two-dimensional negative refractive index plasmonic metamaterials and metamaterial-based nanophotonic devices, which are reasonably easy to fabricate and study. These optical metamaterials and devices may be used in improved microscopy, waveguiding, and laser cavity schemes, which are supposed to exhibit spatial resolution down to $\lambda/7$ level or better. These applications are possible because of the improved figure of merit of the 2D negative refractive index materials operating in the visible frequency range compared to their 3D counterparts. However, losses in these materials remain an important performance-limiting issue.

ACKNOWLEDGMENT

This work has been supported in part by the NSF under Grants No. ECS-0304046 and No. CCF-0508213.

[1] J. B. Pendry, Phys. Rev. Lett. **85**, 3966 (2000).
[2] N. Fang, H. Lee, C. Sun, and X. Zhang, Science **308**, 534 (2005).
[3] D. O. S. Melville and R. J. Blaikie, Opt. Express **13**, 2127 (2005).
[4] I. I. Smolyaninov, J. Elliott, A. V. Zayats, and C. C. Davis, Phys. Rev. Lett. **94**, 057401 (2005).
[5] A. V. Zayats, I. I. Smolyaninov, and A. Maradudin, Phys. Rep. **408**, 131 (2005).
[6] I. I. Smolyaninov, C. C. Davis, J. Elliott, G. A. Wurtz, and A. V. Zayats, Phys. Rev. B **72**, 085442 (2005).
[7] S. A. Ramakrishna and J. B. Pendry, Phys. Rev. B **69**, 115115 (2004).
[8] Z. Jakob, L. V. Alekseyev, and E. Narimanov, Opt. Express **14**, 8247 (2006).
[9] A. Salandrino and N. Engheta, Phys. Rev. B **74**, 075103 (2006).
[10] I. I. Smolyaninov, Y. J. Hung, and C. C. Davis, Science **315**, 1699 (2007).
[11] Z. Liu, H. Lee, Y. Xiong, C. Sun, and X. Zhang, Science **315**, 1686 (2007).
[12] V. M. Shalaev, Nat. Photonics **1**, 41 (2007).
[13] S. Guenneau, A. C. Vutha, and S. A. Ramakrishna, New J. Phys. **7**, 164 (2005).
[14] S. Guenneau, B. Gralak, and J. B. Pendry, Opt. Lett. **30**, 1204 (2005).
[15] S. A. Maier, S. R. Andrews, L. Martin-Moreno, and F. J. Garcia-Vidal, Phys. Rev. Lett. **97**, 176805 (2006).
[16] I. I. Smolyaninov, Appl. Phys. A: Mater. Sci. Process. **87**, 227 (2007).